Raman scattering due to interface optical phonons in GaAs/AlAs multiple quantum wells

A. J. Shields
Toshiba Cambridge Research Centre, 260 Science Park, Milton Road, Cambridge CB4 4WE, United Kingdom

M. P. Chamberlain, M. Cardona, and K. Eberl
Max-Planck-Institut für Festkörperforschung, Heisenbergstrasse 1, D70569 Stuttgart, Germany
(Received 19 January 1995)

We present measurements and calculations of the resonant Raman line shape due to optic phonons in GaAs/AlAs multiple quantum wells (MQW's). Under resonant photoexcitation conditions we observe broad features between the bulk LO and TO frequencies in *both* the GaAs and AlAs optic phonon regions, due to modes propagating in the layer plane (in-plane modes). These are much stronger for the outgoing than the incoming resonance condition due to relaxation of the photoexcited exciton to states of the finite in-plane center-of-mass wave vector. The broad feature in the GaAs region displays a number of dips that can be assigned to the anticrossing of the interface dispersion with odd-order confined modes. We present a macroscopic model for calculating the resonant Raman line shape that incorporates the coupling to the in-plane modes, described realistically as combinations of interfacelike and confinedlike parts. Calculated line shapes reproduce closely the spectra measured for several MQW's of differing layer widths. In particular, good agreement is found for the dependence of both the GaAs and AlAs optic phonon regions on the AlAs thickness, which provides convincing proof of the role of interface modes in the spectra.

I. INTRODUCTION

The layering of the dielectric constant in polar semiconductor heterostructures results in the frequency of their infrared-active, optical phonons being strongly dependent on the propagation direction. This arises essentially from the variation of the electrostatic restoring force responsible for the LO-TO splitting on the wave vector orientation. As a consequence, the LO and TO vibrations converge to a common intermediate frequency with increasing in-plane wave vector (q_x). This band of phonon modes between the LO and TO frequencies, widely referred to as *interface modes*, is known to be responsible for the broad feature seen in the AlAs region of resonant Raman spectra of GaAs/$Al_xGa_{1-x}As$ multiple quantum wells (MQW's) and superlattices (SL's).[1-3] Since these Raman spectra were recorded with the incident and scattered light propagating normal to the layer planes, so that the in-plane wave vector transferred to the phonon (q_x) by the light is zero, observation of the interface modes required the involvement of an additional elastic scattering mechanism in the Raman process.

Confinement of the optic vibrations to individual layers in MQW's arises when the phonon frequencies of the constituent materials differ considerably, preventing the optic modes from propagating from one layer to the next. For instance, the confined modes obtained in GaAs/AlAs MQW's, where the bulk AlAs LO and TO frequencies are $\approx 100\ \mathrm{cm}^{-1}$ higher than those of GaAs, due to the lighter cation mass of AlAs. For $q_x = 0$, the normal modes are analogous to those of a vibrating string with fixed ends, with quantized wave vector along the normal to the layers (z direction) given by

$$Q_z = \frac{m\pi}{d_1 + \Delta}\ , \tag{1}$$

where m is an integer called the mode order, d_1 is the confining layer thickness, and Δ is the penetration of the vibration into the barrier. Since the vibration usually extends to the first cation plane in either barrier, beyond the interface boundary defined by the anion plane, $\Delta = 1$ monolayer (ML). As the wave vector along the z direction need not be conserved in the scattering process, a number of peaks are observed in the Raman spectra, corresponding to modes of different order (m), labeled LO_m and TO_m for the longitudinal and transverse vibrations, respectively.[1,4-12] Several works have demonstrated that the frequencies of these so-called *confined* phonons, plotted against their effective wave vector due to confinement, given by Eq. (1), roughly map onto the bulk optic dispersions.[1,6,8,10]

There has been a great deal of theoretical interest in the dispersion of the confined modes away from $q_x = 0$. Microscopic calculations[13] showed that the confined phonons with $m = odd$ disperse strongly with q_x and anticross with one another, while, in contrast, the even-order modes are almost dispersionless. The interface mode dispersions calculated after neglecting confinement effects, pass through the anticrossings of the odd-order branches. Macroscopic models[14,15] described the MQW phonons as a mixture of confined and pure interface parts, which together satisfy both the mechanical and electrostatic boundary conditions. While the macroscopic approach could reproduce the dispersions calculated by the more rigorous microscopic models,[15] they also provide considerable insight into the origin of the rather complex dispersion.

Experimental confirmation of the strong dispersion of the confined modes has come from nonresonant Raman spectra taken with the light incident on cleaved and polished edges of the layers, which induces an in-plane phonon wave vector.[16,17] The experimentally measured dispersion was shown to be well reproduced[17] by the macroscopic phonon model[15] that we have employed in this paper. We demonstrate here that, thanks to a breakdown in the wave vector conservation rule under resonant photoexcitation conditions, this complex dispersion of phonons in MQW's also determines the structure in resonant spectra recorded in the more usual geometry with the light propagating normal to the layers.

The selection rules regarding which orders are observable in Raman spectra are governed by the parity of the modes, with respect to the reflection plane bisecting the well. The scattering amplitude for each confined mode is determined by the electron-phonon interaction matrix element,

$$M(m) = \int_{-\infty}^{+\infty} \psi^*(z)\chi_m(z)\psi(z)\, dz \; , \qquad (2)$$

where $\psi(z)$ and $\chi(z)$ are the envelope functions that describe, respectively, the electron wave function and phonon potential along the z direction. Since the electron probability density, $|\psi(z)|^2$ is, to a good approximation, symmetric about the plane bisecting the well [this symmetry is exact with respect to the twofold rotations with respect to the axes (1, $\pm$ 1, 0) perpendicular to z], $M(m) = 0$ for those modes with antisymmetric interaction potential $\chi(z)$. The atomic displacements, $u_m(z)$, of the odd- and even-order GaAs confined phonons are symmetric and antisymmetric about the center plane of the well, respectively, as apparent by analogy with the normal modes of a vibrating string with fixed ends. For the deformation-potential interaction, which dominates under nonresonant photoexcitation conditions, $\chi_m(z) \propto u_m(z)$, so that $M(m = \text{even}) = 0$, thus producing a finite coupling for the odd modes alone. On the other hand, for the Fröhlich interaction, the atomic displacement produces an electric field (E_m), the scalar potential (χ_m) associated with which satisfies, $-\frac{\partial \chi_m}{\partial z} = E_m \propto u_m$. This results in the Fröhlich interaction potentials having opposite symmetry to those of the deformation-potential interaction and produces finite scattering strength only for the even modes.

Evidence supporting these selection rules was presented by Sood *et al.*[6] They observed only the odd-order modes for nonresonant conditions and, conversely, peaks at even-mode frequencies under resonant photoexcitation. They argued that under resonant conditions, the strong increase in the Fröhlich interaction results in it dominating over the deformation potential. Since then numerous other authors (see, for example, Refs. 1, 3, 6–12) have assumed the resonant Raman spectrum to consist of a series of peaks, due to the even-order confined modes.

Recently we demonstrated that the above, widely accepted interpretation of the resonant Raman spectrum as a series of peaks due to even-order confined modes is incorrect.[18,19] In fact, the interface modes are the origin of most of the Raman intensity in the GaAs region, apart from a strong peak due to LO_2. The interface modes produce a broad feature between the LO and TO frequencies in the GaAs optic region, as in the AlAs region. However, in the GaAs region the interface feature has a number of minima, due to anticrossings of the interface branches with the odd-order confined modes, which produces gaps in their dispersions. The maxima between these minima lie (coincidentally) close to the frequencies of the even modes, but do not derive from scattering by the even-order modes. The intensities of the even-order modes decreases monotonically with mode order, so that they are too weak to be seen above the contribution of the interface mode. Other authors have considered nonresonant Raman scattering theory in GaAs/AlAs superlattices, using an effective bond orbital method. However, a simplified phonon model is used, derived from a rigid-ion model, where the modes are assumed to only have wave vectors along the growth direction.[20] A detailed microscopic theory of Raman scattering in quantum well structures has also been performed, where the phonon modes are considered as separate noninteracting sets of confined and interface modes.[21] Neither of these models describe the mixing of the confined and interface modes which takes place at finite in-plane wave vector (q_x), but we demonstrate in this publication that the treatment of this mixing is essential in order to understand our recent resonant Raman scattering experiments.

In this paper, we present a model for calculating the resonant Raman line shape, due to optic phonons in polar MQW's, which we compare to our measurements. In the following section, we present experimental spectra and briefly summarize its correct interpretation. A model, which uses realistic phonon potentials for the electron-phonon interaction when calculating the resonant line shape, is presented in Sec. III. In Sec. IV, we compare the results of the calculations to Raman spectra measured in GaAs/AlAs MQW's of differing layer dimensions. The difference in the Raman line shape of the GaAs modes for incoming and outgoing resonance, their dependence on AlAs layer widths, and the spectra of the AlAs modes is well reproduced by our calculations and supports our interpretation of the line shape.

II. EXPERIMENTAL RAMAN LINE SHAPES

A. Experimental results

We have measured Raman spectra of a number of GaAs/AlAs MQW's with different layer widths, grown by molecular beam epitaxy on (100) oriented GaAs substrates. The four samples had MQW's with layer widths of 45/22, 46/46, 51/46, and 43/85 Å determined by x-ray crystallography to an accuracy of 1 ML ($\pm$ 2.83 Å). The samples were cooled to a temperature of 10 K for the resonant measurements, while the nonresonant spectra were recorded at 80 K. Raman spectra were taken in the nearly backscattering geometry, with the incident and scattered light propagating almost normal to the layer planes (z direction) and polarized along the principal crystal axes (x and y). A tunable Ti-sapphire laser induced the resonant spectra, while the discrete lines of an argon-ion laser were employed for the nonresonant measurements.

Figure 1 plots Raman spectra measured on the 46/46 Å GaAs/AlAs MQW with the 488 nm line of the argon-ion laser, the energy of which is away from any strong critical points in the band structure. A series of peaks are observed in the crossed polarization geometry, $z(x,y)\bar{z}$, due to confined phonons with odd-mode order. No structure was resolved for the parallel geometry, $z(x,x)\bar{z}$. The inset shows the Raman shifts of the peaks plotted against their effective wave vector due to confinement, given by Eq. (1), where it can be seen that the points map closely onto the bulk GaAs LO dispersion.[22] The horizontal bars indicate the systematic error caused by inaccuracy of the GaAs layer width measured by x-ray crystallography of one monolayer. The polarization of the Raman signal, in addition to mode-order selection rule, is consistent with scattering due to the deformational-potential interaction, which dominates under nonresonant conditions. Notice that the intensities of the peaks decrease monotonically with mode order, as expected for deformation-potential-induced scattering.

When the laser energy is tuned to energies around the MQW band gap, the LO Raman intensity increases by several orders of magnitude, due to the resonant enhancement of the Fröhlich interaction, as discussed in detail in Refs. 23 and 24 for the 51/46 Å MQW. The strongest Raman scattering is observed, when the scattered photon energy is close to that of the bound exciton formed between the lowest electron and heavy-hole subbands, i.e., outgoing resonance with $e1-\mathrm{hh}1(1s)$. Weaker maxima are observed for incoming resonance with $e1-\mathrm{hh}1(1s)$, when the incident photon energy is tuned to the MQW band gap and also for outgoing resonance with the light-hole exciton, $e1-\mathrm{lh}1(1s)$.

The Raman line shape measured under resonant photoexcitation is completely different from that for nonresonant conditions, as can be seen in Fig. 2, which compares spectra recorded for outgoing resonance with $e1-\mathrm{lh}1(1s)$ and incoming resonance with $e1-\mathrm{hh}1(1s)$. In this figure, the spectra are recorded for parallel polarization, $z(x,x)\bar{z}$. For $z(y,x)\bar{z}$, we measured very similar line shapes, with typically about half the strength of the parallel geometry. The strong photoluminescence[23] of the $e1-\mathrm{hh}1(1s)$ transition prevents accurate measurement of the Raman line shape for outgoing resonance with $e1-\mathrm{hh}1(1s)$. However, the nature of the exciton has little influence on the Raman spectrum, since line shapes measured on the high-energy side of the $e1-\mathrm{hh}1(1s)$ outgoing resonance are very similar to those recorded for the $e1-\mathrm{lh}1(1s)$ outgoing resonance. There was also no vari-

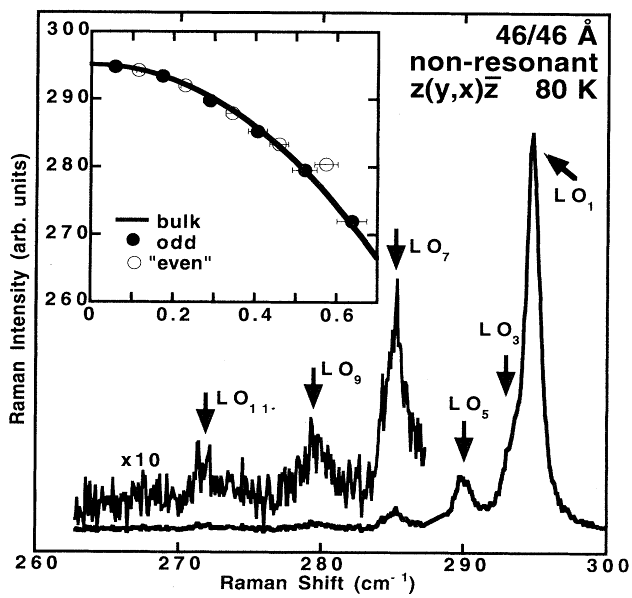

FIG. 1. Raman spectrum taken on a 46/46 Å GaAs/AlAs MQW at 80 K in $z(y,x)\bar{z}$ polarization, with 2.54 eV laser line, corresponding to nonresonant photoexcitation conditions. The peaks are due to odd-order confined modes. The frequencies of these peaks are plotted against their effective k vector, due to confinement (solid symbols) in the inset, which map the bulk GaAs LO dispersion (solid lines). Also plotted (open symbols) are the frequencies of the peaks in the outgoing resonant spectrum, assuming (incorrectly) that they are due to even-order modes.

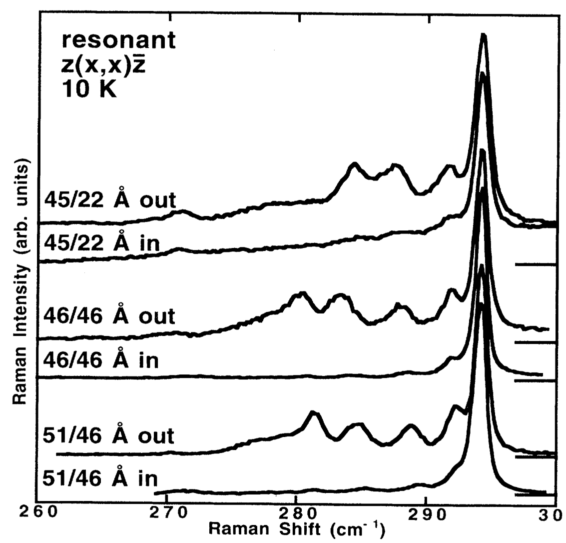

FIG. 2. Comparison of the GaAs optic phonon region of Raman spectra taken for the outgoing and incoming resonance conditions. Spectra taken on MQW's with different layer dimensions (as indicated) are plotted, each recorded for $z(x,x)\bar{z}$ polarization at 10 K. The spectra are normalized to have the same height and are shifted vertically for clarity.

ation in the line shape within each resonance, consistent with the system being inhomogeneously broadened.[23]

Both the outgoing and incoming resonant spectra of Fig. 2 are dominated by the peak due to the LO_2 confined mode. As discussed in Sec. I, the Fröhlich interaction, which dominates under resonant conditions, is expected to couple to only the even-order modes (at in-plane wave vector, $q_x = 0$). We demonstrated recently,[18,19] and discuss briefly in the following section, that the structure in the outgoing resonant spectrum below the LO_2 frequency is due to the interface mode, correcting the previous interpretation of the structure as due to the higher even-order modes. For now, we point out that this interface mode feature is much more prevalent in the outgoing than the incoming resonant spectrum.

Figure 3 shows Raman spectra recorded under the outgoing resonance condition in the region of the GaAs-like optic phonons for each of the MQW's studied. Since the GaAs layer width of the MQW's are similar, we can expect similar GaAs confined-phonon frequencies for each. Notice, therefore, the unexpected dependence of the GaAs-like optic phonon line shape on the AlAs layer thickness. As we discuss later, this is a clear indication that the structure in the outgoing resonant spectra is due to the interface mode. Interface mode features are also observed in the AlAs optic phonon region of the outgoing resonant spectra measured on the MQW's, shown in Fig. 4. The AlAs-like interface modes are not resolved above the photoluminescence background for incoming resonance.

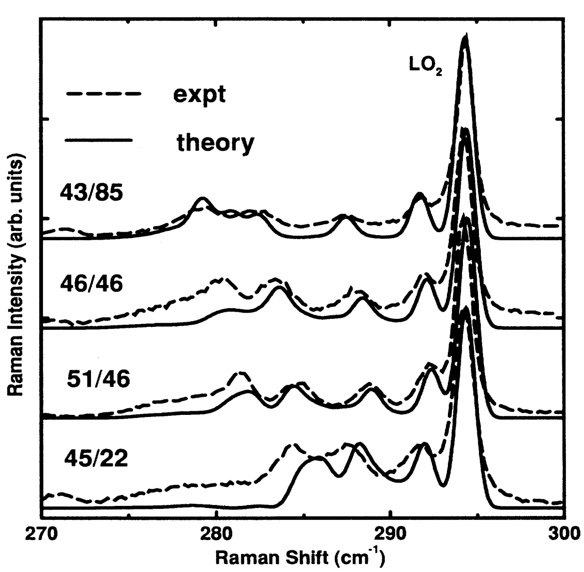

FIG. 3. Comparison of calculated (solid lines) and measured (dashed) Raman spectra due to GaAs-like optical modes of GaAs/AlAs MQW's with differing layer dimensions, for outgoing resonance with $e1 - \mathrm{lh}1(1s)$, at 10 K, in parallel polarization geometry. Spectra are normalized to have the same height and are shifted vertically for clarity.

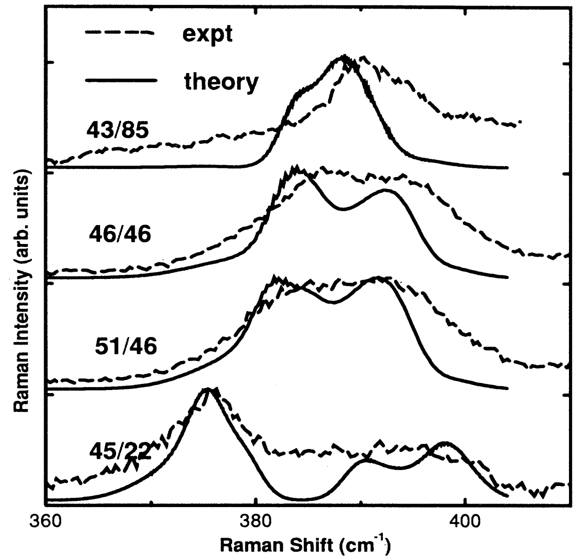

FIG. 4. Comparison of calculated (solid lines) and measured (dashed) Raman spectra of the AlAs-like optical modes of the four GaAs/AlAs MQW's, recorded near outgoing resonance with $e1 - \mathrm{lh}1(1s)$, at 10 K, for parallel polarization geometry.

B. Interpretation of resonant Raman line shape

Two aspects of our experimental data are particularly striking: (1) the line shape due to GaAs-like phonons measured for outgoing and incoming resonance differ considerably, as demonstrated by Fig. 2; and (2) the outgoing resonant line shape depends on the AlAs layer thickness, as shown by Fig. 3. We will demonstrate in this section how these two key findings lead to the correct interpretation of the resonant Raman line shape.

In the experimental geometry used here (and in most Raman experiments on MQW samples), the incident and scattered light propagate almost perpendicular to the layers, so that, for the simplest Raman process, the in-plane wave vector, q_x, imparted to the phonon is zero. This forbids coupling to the interface mode. We suppose that under resonant conditions there is a breakdown of the wave vector selection rule, which occurs by elastic scattering of the photoexcited exciton to finite in-plane center-of-mass wave vectors. Consequently, interface mode features are observed in *both* the GaAs and AlAs optic phonon regions of the Raman spectra under resonant conditions.

The elastic scattering occurs most readily for the outgoing resonance condition, where the photoexcited state is an extended continuum state, as illustrated in Fig. 5. On the other hand, for incoming resonance, where *real* excitation takes place to a bound $1s$ exciton, there is a lack of states at finite in-plane wave vector to elastically scatter to; this process can only be virtual. This explains why the interface feature is observed more strongly for outgoing, than incoming, resonance, for the GaAs-optic

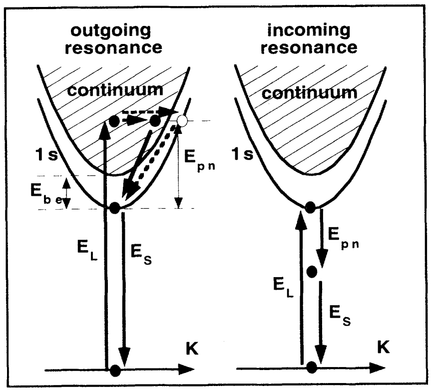

FIG. 5. Schematic of the exciton dispersion showing the laser (E_L) and scattered (E_S) photon energies for the outgoing and incoming resonant conditions. For outgoing resonance, the excitons are photoexcited in the continuum and can, therefore, scatter to finite in-plane center-of-mass wave vectors, $\vec{K}$, providing a coupling to the interface phonons. This explains why the interface modes are observed for outgoing, but not incoming, resonance in Fig. 2.

phonon region in Fig. 2. Similarly in the AlAs region, the interface modes are much stronger for outgoing, than incoming, resonance.

It can be seen that the interface feature observed in the GaAs region displays a number of peaks and dips. This structure arises from the anticrossing of the interface mode dispersion with the odd-order confined modes. The anticrossings produce gaps in the interface dispersion and hence *minima* in the broad interface features at the frequencies of the *odd*-order confined frequencies. The dips in the outgoing resonant spectra coincide with the peaks of the nonresonant spectra, which are also associated with the odd-order confined modes. The lowest-frequency dip derives from a high even-order mode, e.g., LO_8 for the dip near 281.7 cm^{-1} seen in Fig. 3 for the 46/46 Å MQW, which also anticrosses with the interface dispersion away from $q_x = 0$, as discussed in Ref. 15. Similar peaks and dips are not observed in the interface mode features of the AlAs region, because the bulk AlAs LO dispersion is much weaker, with the result that the odd-order LO modes confined to the AlAs are much closer in frequency and not resolved.

With our interpretation, the dependence of the resonant Raman line shape in the GaAs region upon the AlAs layer width can be readily understood. Sood *et al.*[3] have discussed the dependence of the intensity of the interface modes upon the layer widths in terms of the symmetry of the Fröhlich potentials of the upper- and lower-frequency branches for zero phonon wave vector along the z direction. When the AlAs layers are thinner than the GaAs ones, the upper branch of the GaAs-like and the lower one of the AlAs branch have a symmetric potential about the midplane of the GaAs layers and couple strongly in the Raman spectra. On the other hand, for thinner GaAs layers, the lower GaAs-like and upper AlAs-like branches couple in the Raman spectra. Consistent with these arguments, Sood *et al* observed that the maximum of the interface feature of the AlAs optic phonon region is shifted towards lower frequencies for SL's with thinner AlAs layers. Similar behavior can be observed in Fig. 4 for the AlAs region of our MQW's, where the maximum of the interface feature is shifted to lower and higher frequencies for the 45/22 and 43/85 Å structures, respectively. From the above argument, based on the symmetry of the interaction potentials, opposite shifts of the maxima are expected in the GaAs region. This explains why the intensity in Fig. 3 moves out to lower frequencies as the AlAs layer width increases.

The structure in the outgoing resonant spectrum, due to the interface mode, has for several years been misinterpreted as a series of peaks, due to higher ($m = 4, 6, 8...$) even-order confined modes,[1,3,6–12] which, as discussed in Sec. I, couple via the Fröhlich interaction. Since the dips correspond to the odd-order frequencies, the peaks between the dips agree (coincidentally) roughly with the even-mode frequencies, as demonstrated by the open symbols in the inset of Fig. 1. However, it can be seen that the mapping onto the bulk LO dispersion is not so good as for the odd-order modes seen for nonresonant conditions.

The Raman intensities of the confined phonons decrease rapidly with mode order, so that the higher even-order modes are not resolved above the interface mode feature. This arises from the dependence of the Fröhlich interaction potential on the phonon wave vector of $1/q$, resulting in the intensity of the even confined modes decreasing approximately as $1/m^2$. There may, however, be a small contribution to the spectra, due to the LO_4 mode. Clearly the variation in the intensities of the maxima (apart from the LO_2 peak) in the outgoing resonant spectra are not consistent with their origin being a series of peaks, due to even-order modes. If they *were* due to even-order confined modes, we would expect their intensities to decrease monotonically and very rapidly with decreasing frequency, as for the odd-order peaks observed in the nonresonant spectra. In sharp conflict with the expected behavior, the intensities of the maxima in the outgoing resonant spectra increase with decreasing frequency. Furthermore, if the peak near 280.4 cm^{-1} in the outgoing resonant spectrum of the 46/46 Å MQW in Fig. 3 is due to LO_{10}, why is a peak due to LO_{12} not resolved? Ascribing the maxima to even-order modes could also not explain the dependence of the GaAs-like line shape on the AlAs layer thickness, or the difference between outgoing and incoming resonance.

III. MODEL OF RESONANT RAMAN LINE SHAPE

A. Electron-phonon interaction potentials

We use the continuum model of Ref. 15 to describe the optical phonons of the GaAs/AlAs MQW's. We urge readers to refer to Ref. 15, which describes the approach and the calculation of the dispersion relation for the MQW modes. Here, we concentrate on the calculation of the phonon mode potentials, which was not included in the previous publication. The solution of the equation of motion [Eq. (1) in 15] and $\nabla \cdot \mathbf{D}$, where $\mathbf{D}$ is the electric displacement, can be written as a combination of longitudinal optic, transverse optic, and interface modes. Initially, we consider the modes vibrating with frequencies close to those of the longitudinal optic ($\omega_{\rm LO}$) and transverse optic ($\omega_{\rm TO}$) modes of bulk GaAs. Since these GaAs MQW modes vibrate at frequencies $\approx$ 100 cm^{-1} lower than those in the AlAs layers they are, practically speaking, confined to the GaAs layers.[13,15] The displacement of the GaAs modes in the growth direction, z, in the GaAs layer, layer 1, $0\leq z \leq d_1$ can be written as

$$u_z = \Big[q_L\left(Ae^{iq_Lz} - Be^{-iq_Lz}\right) - q_x\left(Ce^{q_0z} - De^{-q_0z}\right) - q_x\left(Fe^{q_xz} - Ge^{-q_xz}\right)\Big]e^{i(q_x\cdot x-\omega t)}. \quad (3)$$

It is apparent that the first term comes from the LO modes, the second from the TO modes, and the final term from the interface modes. The wave vectors q_L, q_0, and q_x are defined in Ref. 15, where they are written as k_L, k_0, and k_x. This is also the case for the definitions of other symbols not explicitly given in this current paper. $A, B, ..., G$ are mode coefficients to be determined by application of boundary conditions at the interfaces. Microscopic models have shown that the displacement of the GaAs modes is zero at the first Al atoms next to the interface,[13] but assuming rigid barriers where the displacement is zero at the interface has proven to be a good approximation.[15] Thus, the displacement of the GaAs modes in the AlAs layer (layer 2), between $z = d_1$ and $z = d_1 + d_2$ is zero. The scalar potential, χ, of the GaAs modes for $0\leq z \leq d_1$ is written:

$$\chi = \Big[i\left(Ae^{iq_Lz} + Be^{-iq_Lz}\right) + s\left(Fe^{q_xz} + Ge^{-q_xz}\right)\Big]e^{i(q_x\cdot x-\omega t)}. \quad (4)$$

One should note that this scalar potential consists of contributions from only the LO and interface modes, because the interaction of the TO modes with electrons via the Fröhlich interaction is negligible.[25] Even though there is no displacement of the GaAs modes in the AlAs barriers there is an electric field, $\mathbf{E}$, ($\mathbf{E}=-\nabla\chi$) in the barriers, which comes from the interface mode component of the MQW modes. For $d_1 \leq z \leq d_1 + d_2$, this is given by

$$\chi = s_{\rm AlAs}\left(He^{q_x(z-d_1)} + Ie^{-q_x(z-d_1)}\right)e^{i(q_x\cdot x-\omega t)} \ . \quad (5)$$

The displacements and potential of the modes in layer 3, the second GaAs layer between $d_1+d_2 \leq z \leq 2d_1+d_2$, can be determined by the use of the MQW Bloch condition that allows us to write the coefficients in layer 3 in terms of those in layer 1. For example, $A_3{=}e^{iq_z(d_1+d_2)}A$, $B_3{=}e^{iq_z(d_1+d_2)}B$, and likewise for the other coefficients. q_z is the global phonon wave vector in the growth direction that induces the phase change of the displacements and potential in subsequent periods of the MQW.

The appropriate boundary conditions are continuity of u_x, u_z, $E_x \propto \chi$, and of $D_z = -E\frac{\partial\chi}{\partial z}$.[15] For the modes of GaAs/AlAs MQW's, the rigid barrier approximation can be used so the first two boundary conditions become $u_x{=}0$ and $u_z{=}0$ at the interfaces instead of being continuous. Applying these four boundary conditions at the two successive interfaces and employing the MQW Bloch conditions, one obtains a set of eight simultaneous equations in the mode coefficients : A, B, C, D, F, G, H, I. The seven coefficients B to I can be determined analytically in terms of the first A, which is incorporated into an overall normalization coefficient $A_{\rm norm}$, to be calculated by canonical energy quantization. Thus, the scalar potential of the GaAs modes in the first GaAs layer is given by

$$\chi = A_{\rm norm}\Big[i\left(e^{iq_Lz} + Be^{-iq_Lz}\right) + s\left(Fe^{q_xz} + Ge^{-q_xz}\right)\Big]e^{i(q_x\cdot x-\omega t)}, \quad (6)$$

where

$$\begin{aligned} F &= \frac{1}{\Delta i}\Big\{f_Lg_xr - f_Z\left(f_L\alpha_+ - g_x\alpha_-\right) + rf_Z^2 \\ &\quad + B\left[g_Lg_xr - f_Z\left(g_L\alpha_+ - g_x\alpha_-\right) + rf_Z^2\right]\Big\} , \\ G &= \frac{1}{\Delta i}\Big\{f_Lf_xr + f_Z\left(f_L\alpha_- - f_x\alpha_+\right) + rf_Z^2 \\ &\quad + B\left[g_Lf_xr + f_Z\left(g_L\alpha_- - f_x\alpha_+\right) + rf_Z^2\right]\Big\} , \\ B &= -\frac{\alpha_{11}}{\alpha_{12}} , \end{aligned} \quad (7)$$

with

$$\alpha_{11} = \frac{q_x^2}{q_Lq_0} + \left[\sinh q_0d_1\left(if_L - pK\right) - \cosh q_0d_1\left(\frac{q_x^2f_L}{q_Lq_0} - qL\right)\right] - \frac{q_x^2}{\Delta q_Lq_0}\left[2f_Lr\cosh q_xd_1 + f_ZP + 2rf_Z^2\right] , \quad (8)$$

$$\alpha_{12} = \frac{q_x^2}{q_Lq_0} - \left[\sinh q_0d_1\left(ig_L + pM\right) + \cosh q_0d_1\left(\frac{q_x^2g_L}{q_Lq_0} - qN\right)\right] - \frac{q_x^2}{\Delta q_Lq_0}\left[2g_Lr\cosh q_xd_1 + f_ZQ + 2rf_Z^2\right] , \quad (9)$$

and

$$\begin{aligned} &\Delta = 4rsf_Zd, \quad f_Z = \exp iq_z\left(d_1 + d_2\right), \\ &f_L = \exp iq_Ld_1, \quad g_L = f_L^{-1}, \quad f_x = \exp q_xd_1 , \\ &g_x = f_x^{-1}, \quad \alpha_+ = \sinh q_xd_2 + r\cosh q_xd_2, \\ &\alpha_- = \sinh q_xd_2 - r\cosh q_xd_2 , \end{aligned} \quad (10)$$

$$\begin{aligned} P &= -2rf_L \cosh q_x d_2 - 2\sinh q_x d_1 \sinh q_x d_2 \\ &\quad -2r\cosh q_x d_2 \cosh q_x d_1 \ , \\ K &= f_Z\left[f_L\left(-f_x\alpha_+ - g_x\alpha_-\right) + 2\sinh q_x d_2\right] \\ &\quad +2rf_Z^2 \sinh q_x d_1 \ , \\ L &= 2f_L r + f_Z[f_L\left(-f_x\alpha_+ + g_x\alpha_-\right) \\ &\quad -2r\cosh q_x d_2] + 2rf_Z^2\cosh q_x d_1 \ , \end{aligned} \tag{11}$$

Q=P, M=K, and N=L, but with f_L replaced by g_L. All other parameters are defined in Ref. 15. Similarly, the scalar potential of the GaAs modes in the AlAs barrier layers is given by

$$\chi = A_{\text{norm}} s_{\text{AlAs}} (He^{q_x(z-d_1)} + Ie^{-q_x(z-d_1)}) e^{i(q_x \cdot x - \omega t)} \ , \tag{12}$$

with

$$\begin{aligned} H &= \frac{1}{2is_{\text{AlAs}}}\Big\{-\left(f_L + Bg_L\right) \\ &\quad +is\left[Ff_x\left(1+r\right) + Gg_x\left(1-r\right)\right]\Big\} \ , \end{aligned} \tag{13}$$

$$\begin{aligned} I &= \frac{1}{2is_{\text{AlAs}}}\Big\{-\left(f_L + Bg_L\right) \\ &\quad +is\left[Ff_x\left(1-r\right) + Gg_x\left(1+r\right)\right]\Big\} \ . \end{aligned} \tag{14}$$

The Hamiltonian of the optical phonons in the MQW represents the total energy of the modes and is written[26]

$$\mathcal{H} = \frac{\epsilon_0}{2}\int \frac{\partial}{\partial\omega}\left(\epsilon_i\omega\right) E^2 d^3 r \ . \tag{15}$$

ϵ_i is the dielectric function of the GaAs (i=1) and AlAs (i=2) layers [Eq. (14) in Ref. 15] and $\mathbf{E}$ the electric field of the optical modes. The derivative of the product $\epsilon_i\omega$, with respect to ω, leads to both the electrostatic and mechanical contributions to the energy. The electric field is given by $\mathbf{E}$=$-\nabla\Xi$, where the phonon potential Ξ is written in its canonical form,

$$\Xi = \int dq_x \int dq_z \left(\chi\mathbf{a} - \chi^*\mathbf{a}^\dagger\right) . \tag{16}$$

$\mathbf{a}^\dagger$ and $\mathbf{a}$ are the phonon creation and annihilation operators and χ is defined by Eq. (6) in the GaAs layers and Eq. (12) in the AlAs layers. In order to determine the normalization coefficient A_{norm}, we use the fact that the Hamiltonian can also be written in its canonical form,

$$\mathcal{H} = \int dq_x \int dq_z \hbar\omega\mathbf{a}^\dagger\mathbf{a}. \tag{17}$$

$\mathbf{a}^\dagger\mathbf{a}$ is the number of phonons of wave vector q_x and q_z. These have energy $\hbar\omega$ and so summing over all wave vectors gives the total energy of the optical modes. The normalization coefficient is then calculated by substituting Eq. (16) in Eq. (15) and equating it to Eq. (17). A_{norm} is then given by

$$\begin{aligned} A_{\text{norm}}^2 \Bigg[\frac{d\left(\epsilon_1\omega\right)}{d\omega} \Big\{ & d_1\left(q_x^2 - q_L^2\right)\left(BS_j^* + B^*S_j\right) + d_1\left(q_x^2 + q_L^2\right)\left(R_j + BB^*\tilde{R}_j\right) \\ & +2q_x \sinh\left(q_x d_1\right) s^2 \left(FF^* e^{q_x d_1} + GG^* e^{-q_x d_1}\right) \\ & +2sq_x\left(-F^*T_j - BG^*\tilde{T}_j + G^*V_j + BF^*\tilde{V}_j + GV_j^* + B^*F\tilde{V}_j^* - FT_j^* - B^*G\tilde{T}_j^*\right)\Big\} \\ & +\frac{d\left(\epsilon_2\omega\right)}{d\omega} 2s_{\text{AlAs}}^2 q_x \sinh\left(q_x d_2\right)\left(HH^* e^{q_x d_2} + II^* e^{-q_x d_2}\right)\Bigg] = \frac{\hbar\omega\left(d_1 + d_2\right)}{8\pi^3\epsilon_0} \ . \end{aligned} \tag{18}$$

In the expression for A_{norm} above, the following symbols are defined as

$$\begin{aligned} R_j &= e^{i(q_L - q_L^*)d_1/2}\frac{\sin\left[(q_L - q_L^*)d_1/2\right]}{\left(q_L - q_L^*\right)d_1/2}, \\ \tilde{R}_j &= e^{-i(q_L - q_L^*)d_1} R_j \ , \\ T_j &= e^{i(q_L - iq_x)d_1/2}\sin\left[(q_L - iq_x)d_1/2\right], \\ \tilde{T}_j &= e^{-i(q_L - iq_x)d_1} T_j \ , \\ V_j &= e^{i(q_L + iq_x)d_1/2}\sin\left[(q_L + iq_x)d_1/2\right], \\ \tilde{V}_j &= e^{-i(q_L + iq_x)d_1} V_j \ , \\ S_j &= e^{i(q_L + q_L^*)d_1/2}\frac{\sin\left[(q_L + q_L^*)d_1/2\right]}{\left(q_L + q_L^*\right)d_1/2}, \end{aligned} \tag{19}$$

and F^* is the complex conjugate of F. We have thus deduced the complete form of the electrostatic potential of the GaAs optical modes in both the GaAs and the AlAs layers. When considering the Raman scattering in Sec. III B, we are at outgoing resonance with the GaAs $e1 - \text{lh}1(1s)$ exciton state and so calculate the exciton-phonon interaction in the GaAs layers, using the potential given by Eq. (6) and Eq. (18). When calculating the Raman intensities of the AlAs phonon modes, we are still at resonance with states in the GaAs and so it is the interaction of the AlAs modes' potential in the GaAs layers that is important. The AlAs phonon modes are modeled in an analogous manner, but the first AlAs layer is defined for $0 \leq z \leq d_1$ and the first GaAs layer for $d_1 \leq z \leq d_1 + d_2$. The same equations as for the GaAs modes can then be used, but with the parameters previously given for GaAs replaced by those for AlAs and those for AlAs replaced by those for GaAs. The exciton phonon interaction for the AlAs phonons in the GaAs layers, now the barrier layers for the AlAs modes, is given by Eq. (12) and Eq. (18), with the parameters for GaAs and AlAs interchanged.

B. Resonant Raman intensity due to optic modes

Light scattering by phonon emission is usually described by a three step process, involving (i) photoexcitation of an electron/hole pair by the incident photon of energy E_L and center-of-mass wave vector $\vec{K}_L$, (ii) inelastic scattering of the electron/hole pair by emission of a phonon of energy $E_{\rm pn}$ and wave vector $\vec{q}$, (iii) recombination of the electron and hole with emission of a photon of energy E_S and center-of-mass wave vector $\vec{K}_S$.

Energy and wave vector conservation dictates $E_L = E_S + E_{\rm pn}$ and $\vec{K}_L = \vec{K}_S + \vec{q}$. In the usual geometry in which Raman experiments are performed on MQW samples, with the incident and scattered light propagating along the direction perpendicular to the layer plane, wave vector conservation requires that the in-plane wave vector transferred to the phonon be zero. This forbids coupling to the interface modes, which by definition have a finite in-plane wave vector. Consequently, in order to obtain a finite intensity for the interface modes, it is necessary to assume that elastic, as well as phonon, scattering takes place. The effect of this elastic scattering is to impart a finite in-plane center-of-mass wave vector to one of the intermediate states. The origin of the elastic scattering is irrelevant to the analysis presented here, but we suggest it could derive from interface roughness, which is well known to cause inhomogeneous broadening in these systems.[12]

The experimental spectra we wish to model are taken under outgoing resonance conditions, where the scattered photon energy is equal to that of the $1s$ exciton with zero in-plane center-of-mass wave vector ($\vec{K}$), as shown schematically in Fig. 5. The photoexcited exciton lies in the exciton continuum and has an energy associated with its relative electron-hole motion equal to ($E_{\rm pn} - E_{\rm be}$), where $E_{\rm be}$ is the binding energy of the $1s$ exciton. Since this continuum state has a spatially extended envelope function, it should have a high probability of being elastically scattered. This facilitates a coupling to phonons with in-plane k vector, $q_x \leq \sqrt{2M\,(E_{\rm pn} - E_{\rm be})}/\hbar$, represented by the solid arrows in Fig. 5. Additionally, elastic scattering to the $1s$ bound state (dashed arrows in Fig. 5) produces coupling to phonons with $q_x = \sqrt{2ME_{\rm pn}}/\hbar$. The total integrated Raman strength for outgoing resonance with the $1s$ exciton can be written

$$\sum_a \left| \frac{\left\langle 0\,|H_{\rm pt}|\,1s,\vec{K}=\vec{0}\right\rangle \left\langle 1s,\vec{K}=\vec{0}\,|H_{\rm pn}|\,a\right\rangle}{E_S - E_{1s} + i\Gamma_{1s}} \right|^2 \times\delta(E_a - E_S - E_{\rm pn}) \ , \quad (20)$$

where $H_{\rm pt}$ and $H_{\rm pn}$ are the Hamiltonians describing the electron-photon and electron-phonon interactions, respectively, and $|a\rangle$ labels the excitonic state induced by the elastic scattering. This approach is a simplified version of previous calculations, which have described the Raman scattering by a four step process, involving one elastic and one phonon scattering event.[12,27–29] It implicitly assumes that the matrix element for the elastic scattering is constant, independent of $|a\rangle$, while ignoring the other constant terms. Alternatively, we can view Eq. (20) as a second-order process, where coherency with the incoming photon is lost due to multiple elastic scattering events, and the occupancy of the initial state $|a\rangle$ is a constant, which is independent of $|a\rangle$. This is rather similar to previous treatments of phonon sidebands in photoluminescence spectra.[30] In the following analysis, we consider separately the two contributions to the intensity where, first, $|a\rangle$ is a bound $1s$ exciton, and, second, where $|a\rangle$ is a continuum state. The other bound excitonic states make a negligible contribution and are ignored.

We adopt a two band approach, where the electron and hole positions are expressed in cylindrical coordinates, (z_e,$\vec{r}_e$) and (z_h,$\vec{r}_h$), respectively. The motion in the xy plane is recast in the center-of-mass frame, $\vec{R} = (m_e\vec{r}_e + m_h\vec{r}_h)/(m_e + m_h)$ and $\vec{r} = \vec{r}_e - \vec{r}_h$, with the total and reduced masses defined as $M = m_e + m_h$ and $\mu = (m_e^{-1} + m_h^{-1})^{-1}$, respectively. The exciton envelope functions are assumed to be separable into parts describing the motion perpendicular (z direction) and parallel to the quantum wells, which is a good approximation provided the well width is much narrower than the exciton diameter. Hence, the envelope functions in Eq. (20) are represented by

$$|a\rangle \;=\; \psi_e(z_e)\;\psi_h(z_h)\;\phi(\vec{r})\;\frac{1}{2\pi}\;e^{i\vec{K}\cdot\vec{R}} \ , \qquad (21)$$

where $\psi_e(z_e)$, $\psi_h(z_h)$, and $\phi(\vec{r})$ are the envelope functions describing the motion of the electron along the z direction, the hole along the z direction, and the in-plane relative motion.

Assuming the electrons and holes to be perfectly confined within the well in the lowest subbands, their envelope functions along the z direction are both given by

$$\psi(z) \;=\; \sqrt{\frac{2}{d_1}}\;\sin\left(\frac{\pi z}{d_1}\right) \ . \qquad (22)$$

For the $1s$ exciton, the relative in-plane motion is given by

$$\phi_{1s}(r) \;=\; \sqrt{\frac{2}{\pi}}\;\frac{1}{a_{\rm ex}}\;e^{-r/a_{\rm ex}} \ , \qquad (23)$$

while for the continuum state, the Coulomb interaction of the electron and hole is ignored, allowing the relative motion to be approximated by another plane wave,

$$\phi_{\vec{k}}(\vec{r}) \;=\; \frac{1}{2\pi}\;e^{i\vec{k}\cdot\vec{r}} \ , \qquad (24)$$

normalized such that $\int\,\phi^*_{\vec{k}'}(\vec{r})\;\phi_{\vec{k}}(\vec{r})\;d^2\vec{r} \;=\; \delta(\vec{k}' - \vec{k})$.

The phonon interaction potential acting on the electron and the hole can be expressed as a product of terms involving the motion perpendicular and parallel to the layers,

$$H_{\rm pn} = \sum_{q_z} \sum_{\vec{q}_x} \left[\chi_{\vec{q}_x}(z_e)\, e^{i\vec{q}_x\cdot\vec{r}_e} - \chi_{\vec{q}_x}(z_h)\, e^{i\vec{q}_x\cdot\vec{r}_h}\right] . \tag{25}$$

The form of Eq. (21) for the exciton envelope function allows the electron-phonon matrix element to be separated into integrals over the perpendicular and in-plane directions,

$$\langle b\,|H_{\rm pn}|\,a\rangle = \sum_{q_z} \sum_{\vec{q}_x} M_z(\vec{q}_x)\, M_r(\vec{q}_x)\, \delta(\vec{K}_a + \vec{q}_x) , \tag{26}$$

$$M_z = \int_0^d \psi^*(z)\, \chi_{\vec{q}_x}(z)\, \psi(z)\;dz , \tag{27}$$

$$M_r = \int \phi_b^*(\vec{r}) \left(e^{i\frac{m_h}{M}\vec{q}_x\cdot\vec{r}} - e^{-i\frac{m_e}{M}\vec{q}_x\cdot\vec{r}}\right) \phi_a(\vec{r})\;d^2\vec{r} . \tag{28}$$

As discussed in Sec. III A, the z dependence of phonon potential $\chi(z)$ can be expressed as a sum of confined-phononlike and interfacelike components. Substituting Eq. (6) into Eq. (27) yields,

$$M_z = M_{\rm cp} + M_{\rm if} , \tag{29}$$

$$M_{\rm cp} = \frac{A_{\rm norm}}{q_L d_1}(e^{iq_L d_1} + B)\frac{1 - e^{-iq_L d_1}}{1 - \left(\frac{q_L d_1}{2\pi}\right)^2} , \tag{30}$$

$$M_{\rm if} = \frac{A_{\rm norm}}{q_x d_1}(F e^{q_x d_1} + G)\frac{1 - e^{-q_x d_1}}{1 + \left(\frac{q_x d_1}{2\pi}\right)^2} . \tag{31}$$

We consider, first, the contribution to the Raman intensity of the process, where the elastically scattered exciton is a $1s$ bound exciton with finite in-plane center-of-mass wave vector, i.e., $|a\rangle = \left|1s, \vec{K}_a\right\rangle$. After some straightforward algebraic manipulation the in-plane integral can be reduced to

$$M_r = \frac{8}{a_{\rm ex}^3}\left(\left[4a_{\rm ex}^{-2} + \left(\frac{m_h}{M}q_x\right)^2\right]^{-\frac{3}{2}} - \left[4a_{\rm ex}^{-2} + \left(\frac{m_e}{M}q_x\right)^2\right]^{-\frac{3}{2}}\right) , \tag{32}$$

and, hence, the Raman intensity can be shown to be proportional to

$$I(\omega) = 2\pi K_{1s}\left(|M_z\,[q_x = K_{1s}, q_z(\omega, q_x = K_{1s})]|^2 \times |M_r(q_x = K_{1s})|^2\;\frac{\partial q_z(\omega, q_x = K_{1s})}{\partial\omega}\right) , \tag{33}$$

where $K_{1s} = \sqrt{2ME_{\rm pn}}/\hbar$.

Turning now to the contribution of the continuum states to the Raman intensity, i.e., $a = |k_a, K_a\rangle$, the in-plane integral of the electron-phonon matrix element can be reduced to

$$M_r = \frac{2}{a_{\rm ex}^2}\frac{1}{\sqrt{2\pi}}\left(\left[a_{\rm ex}^{-2} + \left|\vec{k}_a + \frac{m_h}{M}\vec{q}_x\right|^2\right]^{-\frac{3}{2}} - \left[a_{\rm ex}^{-2} + \left|\vec{k}_a - \frac{m_e}{M}\vec{q}_x\right|^2\right]^{-\frac{3}{2}}\right) , \tag{34}$$

leading to the Raman intensity being proportional to

$$I(\omega) = \int 2\pi q_x\;dq_x\;|M_z(q_x, q_z(\omega, q_x))|^2\;k_c \times \int_{-\pi}^{\pi} d\theta\;|M_r(\theta)|^2\;\frac{\partial q_z(\omega, q_x)}{\partial\omega} , \tag{35}$$

where $k_c = \sqrt{2\hbar^{-2}\mu(E_{\rm pn} - E_{\rm be}) - \mu M^{-1}q_x^2}$, and θ is the angle between $\vec{k}_a$ and $\vec{q}_x$.

To take account of broadening, the calculated spectrum is convoluted with a Lorentzian function L of full width at half maximum γ and unit integrated strength. Hence, the total Raman intensity, including the contributions of both the continuum and the $1s$ states is proportional to

$$I(\omega) = \int_0^{\sqrt{2M(E_{\rm pn}-E_{\rm be})}/\hbar} 2\pi q_x\;dq_x\;k_c \int_{-\pi}^{\pi} d\theta\;|M_r(\theta)|^2 \int_0^{\pi/d} dq_z\;|M_z(q_x, q_z)|^2\;L(\omega, \omega_0(q_x, q_z), \gamma)$$
$$+ 2\pi K_{1s}\int_0^{\pi/d} dq_z\;|M_z(q_x = K_{1s}, q_z)|^2\;L[\omega, \omega_0(q_x = K_{1s}, q_z), \gamma] . \tag{36}$$

IV. COMPARISON OF EXPERIMENTAL AND CALCULATED RAMAN LINE SHAPES

We calculate the Raman spectra taking the following parameters : $\omega_{\rm LO}$=295 cm^{-1}, $\omega_{\rm TO}$=271 cm^{-1}, ϵ_0=12.4, v_L=2.90 $\times$ 10^3 ms^{-1}, v_T=2.00 $\times$ 10^3 ms^{-1}, γ=1 cm^{-1}, $E_{\rm pn}$= 38.6 meV for GaAs; $\omega_{\rm LO}$=404 cm^{-1}, $\omega_{\rm TO}$=360 cm^{-1}, ϵ_0=10.1 v_L=1.24 $\times$ 10^3 ms^{-1}, v_T= 2.18 $\times$ 10^3 ms^{-1}, γ=3 cm^{-1}, $E_{\rm pn}$=52.8 meV for AlAs; m_e=0.067; m_h=0.2; $E_{\rm be}$= 11 meV, and $a_{\rm ex}$=93 Å. The 1s exciton binding energy and extent were calculated variationally for a 46 Å GaAs/AlAs QW. The layer widths taken for the calculation are those determined by x-ray diffraction as discussed in Sec. II A. In order to simulate the penetration of the GaAs confined modes into the barrier, we increase the thickness of the confining layer by one monolayer.[1] We noticed that the agreement with experiment could be improved slightly for the 51/46 Å MQW by decreasing the GaAs layer width by 1 ML, which is roughly the accuracy of the x-ray determination.

The solid lines in Fig. 3 plot the Raman spectra calculated for the four MQW's. The peak near 294.2 cm^{-1} for each MQW is due to the LO_2 mode, while nearly all of the rest of the structure derives from the dispersive regions of the phonon dispersion, i.e., the interface modes. As discussed in Sec. II B, the dips in the spectra at frequencies below that of LO_2 are due to anticrossings of the interface branches with the odd-order confined modes. However, the lowest-frequency dip for each spectrum is due to an anticrossing with a high even-order mode, which has been demonstrated to occur in Ref. 15. Good agreement with the experimental spectra (dashed lines) is immediately apparent. In particular, notice that the calculation reproduces the dependence of the line shape on the AlAs layer width, for which we gave a qualitative argument in Sec. II B.

In Fig. 6(a), the dispersion of the GaAs modes for fixed q_z = 8 $\times$10^5 cm^{-1} and varying q_x is compared to the calculated spectrum for the 45/22 Å sample. One can see that the scattering is predominantly due to the highly dispersive upper *interface* mode, with dips coinciding with the anticrossings where the phonon density of states is reduced. It can also be seen that the scattering due to the lower *interface* mode is negligible for this MQW, as its Fröhlich interaction potential has basically the wrong symmetry to couple to the exciton in the GaAs well.

The spectra calculated (solid lines) for the AlAs optic phonon region are compared with the experimental data (dashed) in Fig. 4. Again the dependence on the AlAs layer thickness is in good qualitative agreement. The AlAs curves in Fig. 4 were calculated with γ = 3 cm^{-1}, which is rather broader than the value taken for the GaAs modes in Fig. 3. However, 3 cm^{-1} is in agreement with the values determined from the AlAs optic phonon lifetimes[31] and broadenings[32] and, furthermore, *ab initio* calculations of anharmonic phonon decay indicate shorter lifetimes for AlAs than GaAs.[33] This is essentially because the AlAs optical modes have a greater probability of decaying into two lower-frequency acoustic modes, whose frequency sum equals that of the optical

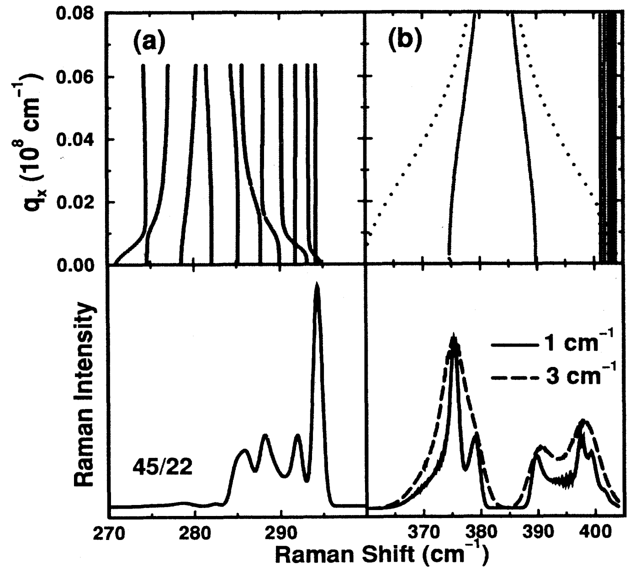

FIG. 6. Calculated Raman spectra of the (a) GaAs and (b) AlAs modes alongside their dispersions for the 45/22 Å MQW. In (a) the dispersion is plotted for q_z=8 $\times$ 10^5 cm^{-1}, while for (b) q_z = 0 (solid lines) or q_z = $\pi/(d_1 + d_2)$ (dotted). The Raman spectra are calculated for γ =1 cm^{-1}, (a) and [(b), solid line], and γ =3 cm^{-1} [(b), dashed line].

mode, because of the accidentally larger density of states of the latter. In GaAs/AlAs MQW's, there is also the added possibility of the AlAs modes decaying into two GaAs modes. The very broad experimental spectra suggests that the AlAs linewidth may be even larger than 3 cm^{-1}.

Notice that, as argued in Sec. II B, the interface features in Fig. 4 have complementary shapes in the GaAs and AlAs phonon regions. For example, for the 45/22 Å MQW, the maximum of the interface feature is shifted to lower frequency in the AlAs region and higher frequency in the GaAs region. On the other hand, the AlAs region differs from the GaAs one in that the minima, due to anticrossing of the interface dispersion with odd-order modes, are not seen since the frequency separation of the AlAs confined modes is much smaller and they are not resolved.

Figure 6(b) plots resonant Raman spectra calculated for the AlAs modes of the 45/22 Å MQW alongside the mode dispersion for the limiting values of q_z = 0 and $\pi/(d_1 + d_2)$ (= 4 $\times$10^6 cm^{-1}). From the upper part of the figure it can be seen that for q_z=0 (solid lines), the interface modes and confined modes are well separated in frequency. For q_z=$\pi/(d_1 + d_2)$ (dotted), the confined modes have basically the same dispersion as before, but the upper interface mode now anticrosses with them. This is barely seen on the figure, due to the closeness of the confined modes to one another, which is a result of the shallow dispersion of the LO phonon in bulk AlAs. No significant Raman intensity occurs due to the AlAs confined modes (i.e., LO_2 or other even m), since their interaction potentials have negligible overlap with the exciton wave function confined mostly to the GaAs layers. Therefore, nearly all the intensity in the AlAs region is due to the interface mode, as already conjectured in Ref. 3. The lower interface branch couples more strongly in the Raman spectrum than the upper one, since it has the more symmetric potential, with respect to the center of the GaAs layers. Notice that, due to the weak bulk AlAs LO dispersion, the confined modes are bunched just below the zone-center LO bulk frequency. Consequently, dips in the Raman intensity due to anticrossing with the odd-order modes, which are so striking for the GaAs modes, are not resolved in the AlAs region. The peaks in the interface feature that can be seen to correspond to maxima in the phonon density of states, which is inversely proportional to $\partial\omega/\partial q_x$. These are seen most clearly for the spectrum in Fig. 6(b), calculated with the narrower linewidth (of 1 cm^{-1}). Increasing the broadening to 3 cm^{-1} smears out these features and gives better agreement with experiment, as shown in Fig. 4.

It is apparent that the spectrum calculated for the 45/22 Å MQW in Fig. 4 shows a gap around 384 cm^{-1}, which is not seen in the experimental spectrum. This gap, which can again be seen in Fig. 6(b), arises from the lack of modes between 379 and 386 cm^{-1} for $q_x \leq 8 \times 10^6$ cm^{-1}, the upper limit of our integration of $q_x = K_{1s}$. At this in-plane phonon wave vector the LO- and TO-like interface branches have not yet converged to their common intermediate frequency. The calculated spectra could, therefore, only be improved by considering phonons of larger q_x. This will arise due to mixing of the light- and heavy-hole excitonic states, which we have ignored and has the effect of providing a coupling to phonons with a larger in-plane wave vector. The mixing of the light- and heavy-hole states is also responsible for the considerable Raman intensity observed for crossed polarization geometry, $z(y,x)\bar{z}$. It is well known that for the simplest Raman process, scattering is only allowed in parallel polarization geometry, $z(x,x)\bar{z}$, for the Fröhlich interaction.[1] However, we can also expect intensity in the crossed geometry if there is relaxation to both light- and heavy-hole states at finite K.[34]

V. CONCLUSIONS

We have presented a method for calculating resonant Raman spectra of GaAs/AlAs MQW's by assuming the photoexcited state relaxes to states of the same energy with finite in-plane wave vector. This elastic scattering is produced by inhomogeneities, such as variations in the layer widths. Our model provides a natural explanation of why we observe phonons of finite in-plane wave vector (i.e., interface modes) for outgoing, but not incoming, resonance. Furthermore, the mixing of the light- and heavy-hole excitonic states away from the Brillouin zone center can account for the depolarization of the Fröhlich-induced scattering observed under resonant conditions.

Our model incorporates realistic electron-phonon interaction potentials, which are a mixture of interface and confined parts. This mixing is responsible for the structure (peaks and dips) seen in the GaAs optic phonon region. The odd-order confined modes anticross with the interface branches and produce corresponding minima in the broad interface feature. On the other hand, the even-order modes do not mix so strongly and have little influence on the spectra, except, of course, for the strong peak due to LO_2. High even-order modes, which do undergo some hybridization, can also produce dips in the interface feature. We have demonstrated, therefore, how resonant Raman spectroscopy provides a method of studying the complicated dispersion of the confined modes away from $q_x = 0$. Since the dispersion of the optical modes in AlAs is very slight, the AlAs confined modes of the MQW's are not greatly separated in frequency and so their anticrossings with the upper AlAs interface mode is not visible in the spectra. The features of the AlAs spectra are also less distinguishable, due to the larger broadening of the AlAs modes.

The dependence of the GaAs-like optic phonon resonant Raman line shape on the AlAs layer width, is particularly convincing proof of the role of the interface modes, since a complementary dependence of the AlAs interface modes on the layer widths is well known.[1,3] Our calculations reproduce the dependence of both the GaAs- and AlAs-like regions on the AlAs layer width and thus confirm our interpretation of the spectra. This interpretation contradicts many previous experimental studies of resonant Raman scattering in MQW's, which now need to be reexamined.

ACKNOWLEDGMENTS

We thank M. Hauser for sample growth, E. Richter and D. Strauch for the bulk phonon dispersion curves, E. Molinari for Ref. 33, B. Jusserand and V. Belitski for interesting discussions, and P. Santos for a careful reading of the manuscript. A.J.S. was funded by the Royal Society (U.K.) and the Max-Planck-Gesellschaft (F.R.G.) and M.P.C. by the European Union. A.J.S. thanks the Max-Planck-Institut for their hospitality during the experimental part of this work.

[1] For a review, see B. Jusserand and M. Cardona, in *Light Scattering in Solids V*, edited by M. Cardona and G. Güntherodt (Springer, Heidelberg, 1989), or J. Menendez, J. Lumin. **44**, 285 (1989).

[2] R. Merlin, C. Colvard, M. V. Klein, H. Morkoc, A. Y. Cho, and A. C. Gossard, Appl. Phys. Lett. **36**, 43 (1980).

[3] A. K. Sood, M. Mendendez, M. Cardona, and K. Ploog, Phys. Rev. Lett. **54**, 2115 (1985).

[4] B. Jusserand, D. Paquet, and A. Regreny, Phys. Rev. B **30**, 6245 (1984).

[5] C. Colvard, T. A. Gant, M. V. Klein, R. Merlin, R. Fischer, H. Morkoc, and A. C. Gossard, Phys. Rev. B **31**, 2080 (1985).
[6] A. K. Sood, M. Mendendez, M. Cardona, and K. Ploog, Phys. Rev. Lett. **54**, 2111 (1985).
[7] A. Alexandrou, M. Cardona, and K. Ploog, Phys. Rev. B **38**, 2196 (1988).
[8] G. Fasol, M. Tanaka, H. Sakaki, and Y. Horikoshi, Phys. Rev. B **39**, 6056 (1988).
[9] T. A. Grant, M. Delaney, M. V. Klein, R. Hondre, and H. Morkoc, Phys. Rev. B **39**, 1696 (1989).
[10] D. J. Mowbray, M. Cardona, and K. Ploog, Phys. Rev. B **43**, 1598 (1991).
[11] D. Gammon, B. V. Shanabrook, and D. S. Katzer, Phys. Rev. Lett. **67**, 1547 (1991).
[12] A. J. Shields, C. Trallero-Giner, M. Cardona, H. T. Grahn, K. Ploog, V. A. Haisler, D. A. Tenne, N. T. Moshegov, and A. I. Toropov, Phys. Rev. B **46**, 6990 (1992).
[13] For example, see E. Richter and D. Strauch, Solid State Commun. **64**, 867 (1987); K. Huang and B. Zhu, Phys. Rev. B **38**, 13 377 (1988); S. Baroni, P. Giannozi, and E. Molinari, *ibid.* **41**, 3870 (1990).
[14] See, for example, B. K. Ridley, Phys. Rev. B **47**, 4592 (1993); C. Trallero-Giner, F. Comas, and F. Garcia-Moliner, *ibid.* **50**, 1755 (1994); H. Gerecke and F. Bechstedt, *ibid.* **43**, 7053 (1991); R. Haupt and L. Wendler, *ibid.* **44**, 1850 (1991).
[15] M. P. Chamberlain, M. Cardona, and B. K. Ridley, Phys. Rev. B **48**, 14 356 (1993).
[16] G. Scamarcio, M. Haines, G. Abstreiter, E. Molinari, S. Baroni, A. Fischer, and K. Ploog, Phys. Rev. B **47**, 1483 (1993).
[17] M. Zunke, R. Schorer, G. Abstreiter, W. Klein, G. Weimann, and M. P. Chamberlain, Solid State Commun. **93**, 847 (1995); *The Physics of Semiconductors*, edited by D. J. Lockwood (World Scientific, Singapore, 1995), p. 947.
[18] A. J. Shields, M. Cardona, and K. Eberl, Phys. Rev. Lett. **72**, 412 (1994).
[19] M. P. Chamberlain, M. Cardona, and A. J. Shields, in *The Physics of Semiconductors*, edited by D. J. Lockwood (World Scientific, Singapore, 1995), p. 907; A. J. Shields, M. P. Chamberlain, M. Cardona, and K. Eberl, *ibid.*, p. 927.
[20] S-F. Ren, Y-C. Chang, and H. Chu, Phys. Rev. B **47**, 1489 (1993); Y-C. Chang, S-F. Ren, and G. Wen, Superlatt. Microstruct. **13**, 165 (1993).
[21] K. Huang, B. Zhu, and H. Tang, Phys. Rev. B **41**, 5825 (1990).
[22] Taken from a 14 parameter shell model fit to neutron scattering data, D. Strauch and B. Dorner, J. Phys. Condens. Matter **2**, 1457 (1990).
[23] A. J. Shields, M. Cardona, R. Nötzel, and K. Ploog, Phys. Rev. B **46**, 10 490 (1992).
[24] A. J. Shields and M. Cardona, in *Coherent Optical Processes in Semiconductors*, edited by R. T. Phillips (Plenum, New York, 1994), p. 313.
[25] M. P. Chamberlain and M. Babiker, J. Phys. Condens. Matter **1**, 1181 (1989).
[26] L. D. Landau and E. M. Lifshitz, *The Classical Theory of Fields* (Pergamon, Oxford, 1975).
[27] W. Kauschke, A. K. Sood, M. Cardona, and K. Ploog, Phys. Rev. B **36**, 1612 (1987).
[28] C. Trallero-Giner, A. Cantarero, and M. Cardona, Phys. Rev. B **40**, 4030 (1989).
[29] A. J. Shields, V. A. Haisler, C. Trallero-Giner, and M. Cardona, in *Phonons in Semiconductor Nanostructures*, edited by J. P. Leburton, J. Pascual, and C. Sotomayor-Torres (Kluwer, Dordrecht, 1993), p. 233.
[30] K. J. Nash and D. J. Mowbray, J. Lumin. **44**, 315 (1989).
[31] A. M. de Paula, A. C. Maciel, M. C. Tatham, and J. F. Ryan, in *The Physics of Semiconductors*, edited by E. M. Anastassakis and J. D. Joannopoulos (World Scientific, Singapore, 1990), p. 1412.
[32] S. Perkowitz, R. Sudharsanan, S. S. Yom, and T. J. Drummond, Solid State Commun. **62**, 645 (1987).
[33] A. Debernardi, S. Baroni, and E. Molinari, in *The Physics of Semiconductors* (Ref. 19), p. 373.
[34] M. Cardona and C. Trallero-Giner, Phys. Rev. B **43**, 9959 (1991).